Rapid Synthesis of [$Au_{25}(Cys)_{18}$] Nanoclusters via Carbon Monoxide in Microfluidic Liquid-Liquid Segmented Flow System and their Antimicrobial Performance

He Huang[a], Gi Byoung Hwang[b], Gaowei Wu,[a] Kersti Karu[b], Hendrik Du Toit[a], Han Wu,[a] June Callison,[c] Ivan P. Parkin[b] and Asterios Gavriilidis[a]*

a: Department of Chemical Engineering, University College London, Torrington Place, London WC1E 7JE, United Kingdom

b: Department of Chemistry, University College London, 20 Gordon Street, London WC1H 0AJ, United Kingdom

c: UK Catalysis Hub, Research Complex at Harwell, Rutherford Appleton Laboratory, Harwell, Oxon OX11 0FA, United Kingdom

Abstract

Atomically precise thiolate-gold nanoclusters with well-defined structures attract attention for use in various applications. However, most of the recently reported synthetic methods rely on prolonged synthesis times (a few hours to days) in order to produce high purity products with a single cluster size. Such extended synthesis times make these processes ill-suited for adaptation to industrial scale production with continuous flow. In this work, an improved method for the synthesis of thiolated Au_{25} nanoclusters is presented utilising a continuous flow microfluidic system and CO-mediated reduction. The optimised system based on a coiled flow inverter with inner diameter of 1 mm operating at 80 °C and 500 kPa took only 3 min for the synthesis of atomically precise cysteine-capped [$Au_{25}(Cys)_{18}$] nanoclusters, as characterised by ultraviolet–visible spectroscopy and electrospray ionization mass spectrometry. The productivity of the system was increased by using higher reactant concenctrations which led to a throughput of 0.9 g_{Au} per day, without changing the reaction time or affecting the product purity. The Au nanoclusters were used as photobactericidal enhancement materials. In antimicrobial testing against *S. aureus,* encapsulation of the Au nanoclusters into crystal violet impregnated silicone showed high photobactericidal activity (~1.7 log reduction in viable bacteria) upon 6 h illumination of white light at ~ 312 lux, while crystal violet did not show significant photobactericidal activity on its own.

Keywords: gold nanoclusters; carbon monoxide reduction; tube-in-tube contactor; coiled flow inverter; Taylor flow; light-activated-antimicrobial-agents

1. Introduction

Atomically precise gold nanoclusters (Au NCs) contain discrete numbers of gold atoms with a defined ligand shell [1]. Due to their small size, they exhibit quantum size effects and have drawn significant attention in recent years due to their unusual molecular-like properties, such as discrete electronic transitions for enhanced optical properties [2], photoluminescence for bio-labels [3], quantized charging for self-assembly control [4] and atomically precise size for catalysis [5]. Among them, thiolated Au NCs ($[Au_n(SR)_m]$), especially $[Au_{25}(SR)_{18}]$ nanoclusters, have been extensively investigated owing to their high thermodynamic stability in the presence of excess thiol ligands [6].

Typically, the Au NCs protected by thiol ligands are produced with the use of a strong reducing agent (such as sodium borohydride, $NaBH_4$) to reduce thiolate-Au(I) complexes [7], which first leads to a mixture of different cluster sizes due to the fast and uncontrolled reduction kinetics akin to the rapid formation of small gold nanoparticles (Au NPs) by similar methods [8]. It has been well established that during this stage, use of lower temperatures (e.g., ice-cold solutions) to suppress the reducing ability of $NaBH_4$ is helpful to control the size distribution of the Au NPs [8, 9]. A similar strategy was also utilized by adding $NaBH_4$ to a thiolate-Au(I) solution at 0°C to produce Au NCs [10]. High purity of $[Au_{25}(SR)_{18}]$, which has the highest thermodynamic stability [7, 11], can be obtained with long aging times under the gentle environment created due to the etching effect by excess thiol ligands [6]. The free thiol can remove the gold atoms from the synthesized $Au_n(SR)_m$ clusters to lead to more stable clusters. As this stage is thermodynamically controlled, the general synthetic time could be a few hours to days in order to leave enough time for cluster size evolution and focusing [12, 13]. During this “size-focusing” stage, heating, which is the most efficient method of energy input, can facilitate the transformation process of mixed size Au NCs into more thermodynamic stable Au NCs of atomic precision and decrease the total reaction time required [14]. Considering the conflicting favourable conditions at different synthetic stages, Qian and Jin used a two-step method to synthesize high purity $[Au_{144}(SCH_2CH_2Ph)_{60}]$ nanoclusters, by a modified Brust-Schiffrin method with a first-stage reduction and a second-stage addition of excess thiol at 80 °C for 24 h for size-focusing [15]. Katla *et al.* developed a one-pot synthesis of $Au_{25}(SG)_{18}$ NCs at an elevated temperature (60 °C) to speed up the aging process and the whole reaction time could be reduced to 2 h [16].

Besides the adjustment of temperature, Xie and co-workers [17] made use of NaOH addition to tame the reducing ability of $NaBH_4$, as well as to increase the etching ability of thiols to synthesize $[Au_{25}(SR)_{18}]$ clusters. They further studied the effect of temperature on

nanoclusters formation and concluded that 40 °C is the optimal temperature for $NaBH_4$ reduction to speed up the reaction rate without further irreversible transformation into mixed size Au NCs under higher temperature [14]. However, using $NaBH_4$ as a reducing agent may bring about boron contamination into the final product, in addition to the inevitable decomposition of $NaBH_4$.

Instead of using $NaBH_4$, Xie and co-workers proposed an allternative reduction approach utilising gaseous carbon monoxide as reducing agent to direct a slow and size-controlled synthesis of $[Au_{25}(SR)_{18}]$, which leads to a highly pure product at room temperature with a 24 h reaction time [11]. The mechanism of $[Au_{25}(SR)_{18}]$ formation by CO reduction was investigated by the same group to show the cluster evolution from Au(I) precursor to final Au_{25} clusters by UV-Vis spectroscopy and electrospray ionization mass spectrometry (ESI-MS) [18]. The first stage, governed by kinetic control, finished in the first 40 min, and reduced most of Au(I) complexes into NCs with Au atoms ranging from 4 to 10. In the remaining time, up to 72 h, the slow "size-focusing" growth was governed by thermodynamic control, converging all the intermediate NCs to $[Au_{25}(SR)_{18}]$ with high purity.

Considering the important role of reaction temperature in the Au NCs synthesis, a microfluidic system was developed for CO-directed $[Au_{25}(Cys)_{18}]$ synthesis in this study, in an attempt to accelerate the thiolated Au NCs synthesis with better quality control. Instead of bubbling CO through the solution, a heptane carrier phase was saturated with the gaseous reducing agent in a tube-in-tube membrane contactor, which offered an enhanced safety platform with fully sealed CO gas inside the outer tube. The transfer of the CO to the gold precursor containing aqueous phase was facilitated by directly contacting the CO-saturated heptane with the aqueous stream, forming segmented flow with high interfacial surface areas in a coiled flow inverter (CFI) made of a capillary with inner diameter of 1 mm. Thus, the controlled addition of CO to the aqueous phase occurred from a high excess CO reservoir. The synthesised $[Au_{25}(Cys)_{18}]$ NCs were utilised for antimicrobial surface preparation. Antimicrobial surfaces is an important application in healthcare environments. There are 2 million incidences of healthcare-associated infections (HAIs) in US hospitals and approximately 90,000 of the patients die by HAIs, which ranks HAIs as fifth leading cause of death in acute-care hospitals of United states (US); 60-70% of HAIs were related to bacterial contamination of hospital surfaces or devices [19, 20].

2. Experimental section

Experimental set-up and procedure for $[Au_{25}(Cys)_{18}]$ nanoclusters synthesis

Figure 1 shows the microfluidic segmented flow system which consisted of a tube-in-tube contactor at room temperature and a coiled flow inverter (CFI) sub-merged inside a stirred glycerol (99.5 %,VWR) bath placed on a hot plate (UC152D with SCT temperature controller, Stuart) for the synthesis of Au NCs at elevated temperature. The tube-in-tube contactor used a 2 m long Teflon AF-2400 tube (0.8 mm inner diameter (ID), 1.0 mm outer diameter (OD), Biogeneral) as the contacting interface placed inside a polytetrafluoroethylene (PTFE) tube (2.4 mm ID, 3.2 mm OD, VICI Jour) and assembled together by two T-pieces (hole size: 1.0 mm, Upchurch). The contactor was used to saturate the heptane, fed by a HPLC pump (P2.1S, Knauer) in the Teflon AF-2400 tube, by CO (BOC gases) that was pressurised in the annulus between the inner and outer tube. A 500 kPa pressure in the CO side was maintained by a gas pressure regulator (K series, Swagelok) and monitored by a pressure sensor (40PC150G, Honeywell) placed at the inlet of the annulus. A coiled flow inverter (CFI) was used as a reactor placed after a T-piece where the organic phase mixed with aqueous solution to form segmented flow to ensure better mixing. The residence time was estimated based on the reactor volume over the total volumetric flow rate of aqueous and organic streams. The chemistry of the synthetic route was based on that reported proposed by Yu *et al.* [11]. The aqueous solution containing $HAuCl_4$ and cysteine (molar ratio, 1:1.5) was prepared using 15.0 MΩ reverse osmosis water with pH tuning to 11.6 by NaOH. All reagents were of analytical grade and purchased from Sigma-Aldrich. The aqueous stream was subsequently pumped into the CFI by a piston pump (milliGAT LF, Global FIA) and merged with CO-saturated heptane at flow ratio of organic to aqueous solution of 2 by a T-mixer (0.5 mm ID, P-632, IDEX) forming microfluidic segmented flow. The CFI was made of fluorinated ethylene propylene (FEP) tubing (1 mm ID, VICI Jour) and consisted of 100 coils with coil diameter of 1 cm. A 90° bend was formed at every 5 coils and the total length of the CFI was 3.6 m (volume 2.83 ml). The outlet of the CFI was connected to a back pressure regulator (BPR-10, Zaiput) connected to a pressure regulator (K series, Swagelok) to maintain the liquid phase pressure at 550 kPa. The solution at the outlet of the back pressure regulator was collected in a glass vial. A gas line of N_2 with volumetric flow rate of 1 ml/min, controlled by a mass flow controller (5850 TR, Brooks), was connected to the glass vial to flush the CO outgassed from the liquid due to decompression. The product was washed and precipitated immediately after reaction with acetone and the precipitate was filtered with a PVDF syringe filter (0.2 µm, Alpha Laboratories) for long term storage. The stability of the solid Au NCs in the fridge was more than 1 month based on the UV-Vis spectrum.

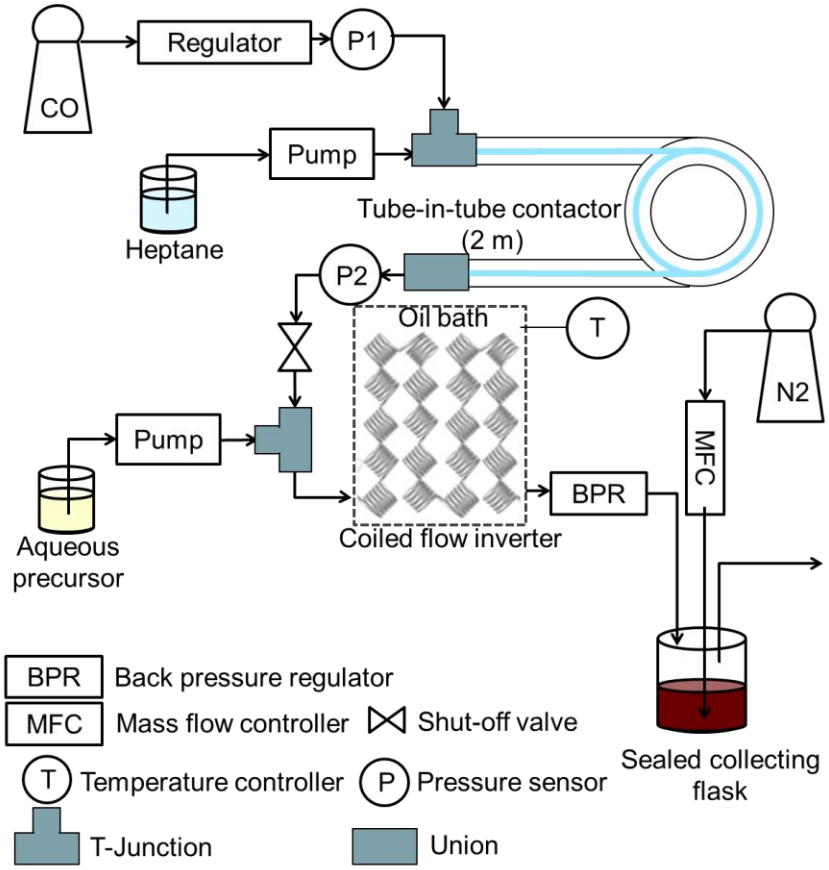

Figure 1. Schematic of the microfluidic segmented flow system developed for synthesis of $[Au_{25}(Cys)_{18}]$ NCs with CO-saturated heptane.

Analysis of $[Au_{25}(Cys)_{18}]$ nanoclusters

The solution pH was measured by a pH meter (pH/Ion S220, SevenCompact™). UV-Vis absorption spectra of the $[Au_{25}(Cys)_{18}]$ solution were recorded using a UV-Vis spectrometer (USB 2000+ spectrometer and DT-Mini-2-GS light source, Ocean Optics). Since in some cases the absorbance values of the synthesised $[Au_{25}(Cys)_{18}]$ solution exceeded the detection limit of this UV-Vis spectrometer, diluted nanocluster solutions were used during measurement and then the data of absorbance peaks were multiplied by the dilution factor to obtain the final UV-Vis spectra. The particle size was also analysed using Small Angle X-ray Scattering (SAXS, Ganesha 300XL, Xenocs/SAXSLAB); the details are shown in the Supporting Information (SI). Microwave Plasma Atomic Emission Spectroscopy (MP-AES, Agilent 4100) was used to measure the gold amount of the synthesized Au NCs after dialysis with a dialysis tube (MWCO 6-8 kDa, Pur-A-Lyzer™). Electrospray ionization mass spectrometry (ESI-MS, Agilent 6510 quadrupole Time-of-Flight (QTOF) mass spectrometer) was used for identifying the mass of the Au NCs. Dried precipitate of Au NCs was diluted in 0.01 µM cesium acetate in water (for operation procedure see the SI). Data acquisition was performed in profile mode

with the mass range from *m/z* 10-10000. Matrix-assisted laser desorption ionization mass spectrum (MALDI-MS, Micromass MALDI-TOF) was also used for verification and also because it offerred wider *m/z* range. The sample was prepared by mixing 2 µL of the raw product with 2 µL of matrix solution (saturated α-cyano-4-hydroxycinnamic acid (CHCA) solution in methanol) and allowed to recrystallize in air prior to the analysis. The data were collected in linear mode. The dried nanoclusters were also analysed by ATR-FTIR spectroscopy using a Perkin-Elmer 1605 FTIR spectrometer with a resolution of 0.5 cm^{-1} and wavenumber range 0-5000 cm^{-1}.

Bactericidal test

To produce the antimicrobial surface, a swell-encapsulation-shrink process was employed lasting 24 h. Silicone pieces (cut from Bescita New Universal Silicone Desktop Computer Keyboard Cover Skin Protector Film, AX-11, China, with area of 4 cm × 7.5 cm) were immersed in a acetone/DI water solution (volume ratio of 1/1) containing 800 mg/L crystal violet (CV) and 35 mg/L $[Au_{25}(Cys)_{18}]$ NCs. During the swelling process, the CV molecules and $[Au_{25}(Cys)_{18}]$ NCs in the mixture penetrated into the silicone matrix as the polymer swelled. After collection of the polymer from the solution, the silicone shrank and CV molecules and $[Au_{25}(Cys)_{18}]$ NCs remained within the polymer matrix. Two samples of $[Au_{25}(Cys)_{18}]$ NCs obtained at 1-day and 3-days of continuous operation of the set-up were used. The details of specific sample preparation are shown in the SI. The antimicrobial activity of control and treated silicone samples were tested against *Staphylococcus aureus* 8425-4 in white light. The light intensity of the white lamp was ~ 312 lux on average. One of the bacterial colonies grown on Mannitol salt agar (Oxoid Ltd) was inoculated into Brain-Heart-Infusion broth (BHI broth, Oxoid Ltd) and cultured in a shaking incubator (200 rpm) at 37 ^{o}C. After 18 h incubation, the bacteria were collected by centrifugation (5000 rpm), washed by 10 ml of phosphate buffer saline (PBS), and then centrifuged and washed to get bacteria resuspended in 10 ml of PBS. *S. aureus* suspension was diluted to get 2.1×10^5 CFU/ml. 25 µl of the bacterial suspension was inoculated onto the treated samples and then the samples were placed in a petri dish with wet paper. The samples were exposed to the white light source for 6 h and then they were located in 450 µl of PBS and vortexed for 30 s. After a serial dilution, 100 µl of bacterial suspension was plated onto Mannitol salt agar and incubated at 37 ^{o}C for 24 h. The bacteria colonies grown in the agar were counted. Statistical t-test of experimental date was performed using Microsoft Excel.

3. Results and Discussion

Adaptation of the synthetic process from batch to flow

To the best of our knowledge, the single-step synthesis of atomically precise Au_{25} NCs in continuous flow has not been investigated. This might be because the prolonged "size-focusing" time of up to several days is hard to adapt to a flow system. The current challenge is in achieving good control of the fast reduction stage, as well as to facilitate the slow size evolution into atomically precise Au_{25} NCs in one stage synthesis (or indeed one tube or microfluidic chip). Based on these considerations, the relatively mild reducing agent CO, was chosen in order to better control the first 'fast reduction' stage instead of cooling reactants as favoured by other researchers. A tube-in-tube contactor was employed to saturate an organic carrier with CO. Based on Henry's law, the amount of dissolved gas in the liquid at equilibrium is proportional to its partial pressure in the gas phase [21]. Therefore the concentration of CO could be tuned by pressurising the microfluidic system. Heptane, which boasts a higher CO solubility (nearly 10 times) than water [22], could act as a CO reservoir to continuously provide reducing agent to the aqueous segments. The CO concentration profile in heptane was calculated using COMSOL (see SI) [23]. The simulation showed that the 2 m Teflon AF-2400 tube was enough to saturate the heptane with 58.4 mM final concentration of CO at 500 kPa. This is signicantly higher than the CO amount required to reduce the gold precursor (0.16 mol of CO per mol of gold precursor) [18] for all experimental condtions employed in this work. Additionally, the CFI provided a compact way of coiling the reactor, having the potential to enhance the mixing between the liquid phases [24]. Thus, the reaction could be precisely controlled as each segment could be regarded as an individual reactor and nearly identical reaction conditions (flow pattern with average aqueous droplet length ~ 2.5 mm and heptane slug length ~4.5 mm (see **Figure S3**).

A preliminary study for the adaptation of synthesis from batch to flow was conducted at room temperature to investigate this liquid-liquid segmented flow system for the $[Au_{25}(Cys)_{18}]$ NCs synthesis without the application of any heat. The UV-Vis spectra of the products at different residence times (obtained by varying the flow rates with constant organic to aqueous flow ratio of 2) are shown in **Figure 2**. Unlike the single absorption peak observed with larger Au NPs (caused by surface plasmon resonance), the nanoclusters, which more closely resemble molecules [25], have quantized energy levels from electronic transitions, and thus exhibit multiple absorption bands in UV–Vis spectroscopy [26]. The typical spectrum of thiolated Au_{25} NCs exhibits four peaks at the wavelengths of 400, 450, 670 and 770 nm, respectively [11]. The pronounced lift of the peak at 670 nm is typically used to determine whether the reaction has reached completion [14]. Yu et al. showed that the thiolate-Au(I) complexes could be fully reduced into Au NCs with mixed sizes during the first 0.5 h of reaction [27], which is the required time for the first 'fast reduction' phase of reaction. The peak at 670 nm gradually appears after the second stage of slow "size-focusing" growth due to the increasing

concentration of Au_{25} NCs. In **Figure 2**, a weak absorbance peak at 670 nm was observed after 0.25 h in our microfluidic set-up. The absorption continued to increase with increasing residence time, indicating the increasing yield of Au_{25} NCs. At residence time of 2 h, a substantial absorption peak at 670 nm wavelength was observed. A 48 h reaction time was achieved by stopping the droplet flow in the CFI. Compared to the peak absorbance at 48 h, the absorbance at 2 h was slightly lower, which indicated the slightly lower yield of $[Au_{25}(Cys)_{18}]$. Nevertheless, this preliminary trial of the adaptation for the synthesis of $[Au_{25}(Cys)_{18}]$ from batch to flow proved to be promising even without applying heat.

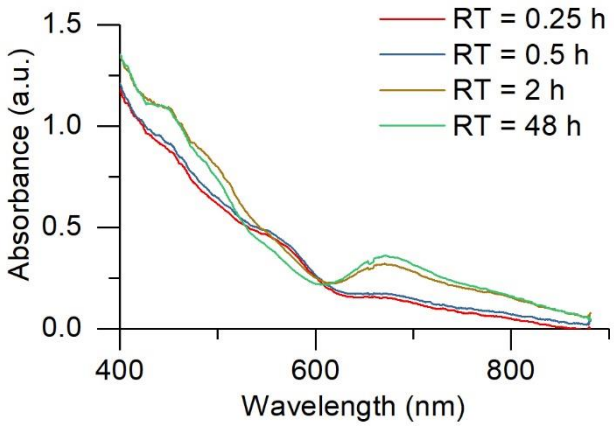

Figure 2. UV-Vis spectra of samples obtained with 1 mM initial concentration of $HAuCl_4$ at room temperature and different residence times (RT) by tuning the flow rates of aqueous and organic streams with constant organic to aqueous flow ratio of 2 and cysteine to gold precursor concentration ratio of 1.5.

Influence of temperature

Even though the preliminary study demonstrated the feasibility of the Au_{25} NCs synthesis in flow, a reaction time of more than 2 h is still unfavourably long for continuous flow synthesis. Since heating has been demonstrated to increase the formation rate of Au_{25} NCs when using $NaBH_4$ as reducing agent [14], experiments were carried out at a residence time of 15 min, but under different elevated temperatures in the range 60 - 120 °C. The UV-Vis profiles of the synthesized products are shown in **Figure 3**. Slightly higher absorbance at 450 nm was observed for the product obtained at 80 °C as compared to that at 60 °C, suggesting higher concentration of Au_{25} NCs. When the temperature was increased to 100 and 120 °C, no absorbance peak was observed at 670 nm, which indicates the formation of multiple cluster sizes as suggested in previous literature [14]. Based on UV-Vis profiles, heating was demonstrated to accelerate the formation of Au_{25} NCs when using CO as reducing agent, and

80 °C was chosen as the optimal reaction temperature. Under this temperature the total reaction time could be decreased to 15 min whilst maintaining the high purity of $[Au_{25}(Cys)_{18}]$.

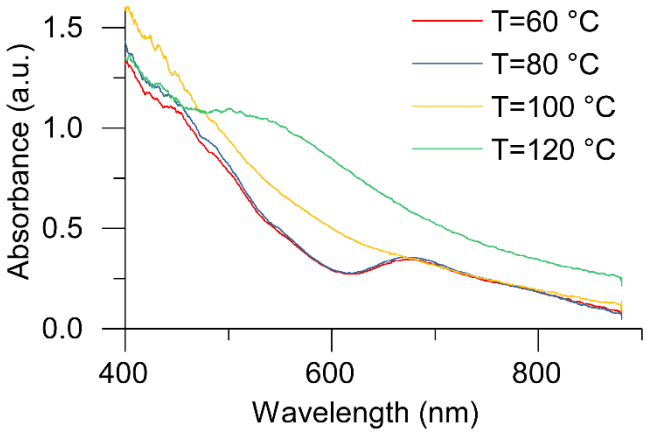

Figure 3. UV-Vis spectra of Au nanoclusters produced using 1 mM $HAuCl_4$ at different reactor temperatures. Residence time 15 min, aqueous flow rate 0.064 ml/min, organic to aqueous flow ratio 2 and cysteine to gold precursor concentration ratio 1.5.

Increase of productivity of the continuous flow system

Increase of productivity of the continuous flow system for the $[Au_{25}(Cys)_{18}]$ synthesis was first investigated by increasing the flow rate (i.e., decreasing residence time in the range 1.5-5.2 min). The product quality could be influenced if the residence time is too short to complete the synthesis. Thus, our aim was to find the shortest residence time without affecting the product quality. When increasing the flow rate, the output solutions became turbid and could not be analysed directly by UV-Vis (shown in **Figure 4a**). The turbidity was due to the significant mixing capability of segmented flow regimes inside CFIs (proven by comparable experiment using a wide coil tube instead of CFI, see the SI) resulting in the heptane forming microdroplets inside the aqueous phase. To precipitate the clusters and terminate the size evolution the sample at the outlet of the reactor was immediately mixed with acetone solution. After collection, it was subsequently filtered with a PVDF syringe filter (0.2 µm pore size) and then re-dissolved in the appropriate amount of water to maintain the same concentration for further characterization. The results of UV-Vis show that the peak absorption at 670 nm wavelength is nearly identical for the different residence times considered. The residence time of 2.9 min was finally chosen as the optimal residence time, as it gave a better defined absorption peak, which indicated the maximum amount of the Au_{25} NCs produced [18].

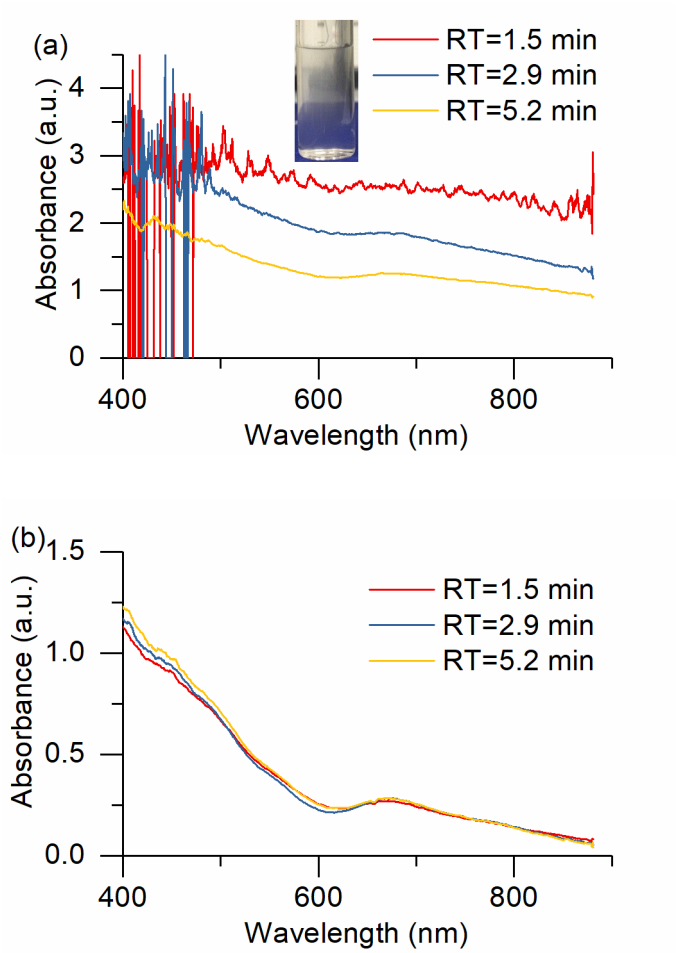

Figure 4. UV-Vis spectra of Au nanoclusters produced using 1 mM $HAuCl_4$ at different residence times (RT), recorded (a) immediately after collection and (b) after washing/precipitating and re-dissolving the clusters. Reactor temperature 80 °C, organic to aqueous flow ratio 2 and cysteine to gold precursor concentration ratio 1.5. The insert in (a) is the cloudy solution formed from DI water and heptane segmented flow at a residence time of 2.9 min.

Next, it was attempted to further increase the productivity of the continuous flow system by increasing the Au precursor concentration in the stock solution at constant concentration ratio of cysteine to $HAuCl_4$ of 1.5. The product collected at the outlet of the reactor was treated immediately with acetone to precipitate and wash the clusters and it was subsequently filtered. The clusters obtained were re-dissolved in DI water for UV-Vis measurement. As the absorbance value of synthesised $[Au_{25}(Cys)_{18}]$ solution exceeded the linear detection range of the UV-Vis spectrometer, a diluted solution was used in this measurement and the data were multiplied by the dilution factor to produce **Figure 5a**. The sharp absorption peak at 670 nm indicated the high concentration of $[Au_{25}(SR)_{18}]$ with increasing initial concentration of gold precursor. There was a red shift of the peak observed (**Figure 5b**) when the initial

concentration of $HAuCl_4$ was over 10 mM, which may be due to the formation of larger cluster sizes [10]. Hence, the UV-Vis results showed that the proposed system could produce pure $[Au_{25}(Cys)_{18}]$ with initial $HAuCl_4$ concentration of up to 10 mM.

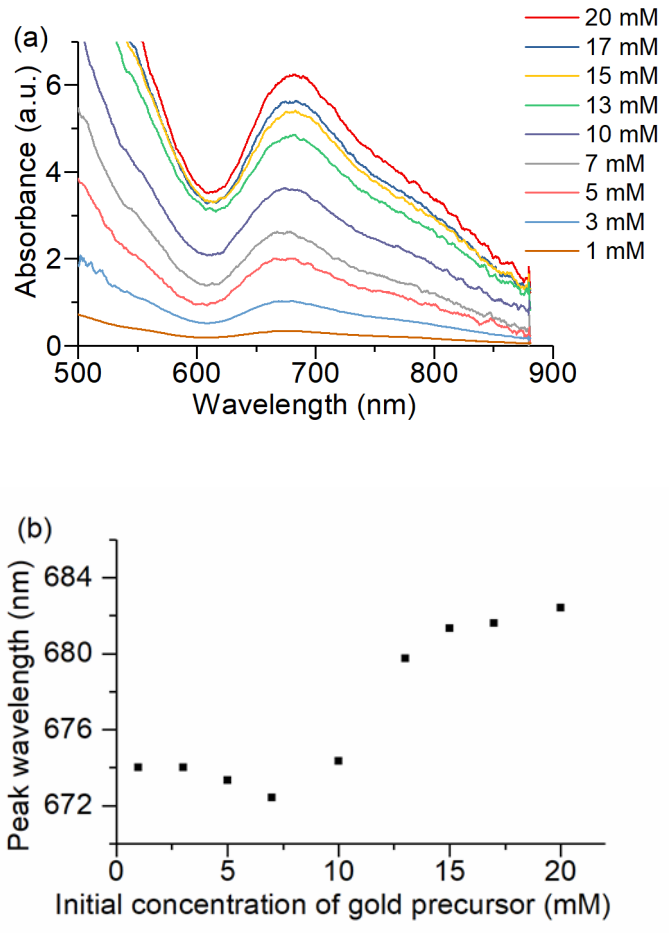

Figure 5 (a) UV-Vis spectra and (b) the exact wavelength of the peak at ~ 670 nm of Au nanoclusters produced using different initial concentration of $HAuCl_4$. Residence time 2.9 min, reactor temperature 80 °C, organic to aqueous flow ratio 2 and cysteine to gold precursor concentration ratio 1.5.

Characterization of the synthesized $[Au_{25}(Cys)_{18}]$ nanoclusters

The particle size of the Au_5 NCs obtained with 10 mM initial gold precursor concentration at 80 °C with a residence time of 2.9 min was analysed by SAXS. The average particle size obtained (see **Figure S5**) was ~1.5 nm. The particle size measured in our work was larger than measured sizes of Au_{25} NCs in organic solvent [30], which could be attributed to ionic strength-dependent aggregation of the gold clusters in water solvent during the 1 h SAXS measurement time [31]. IR spectra did not show the characteristic peak of S-H of the cysteine molecule for the solid Au_{25} NCs (**Figure S6**), indirectky confirming the Au-S interaction.

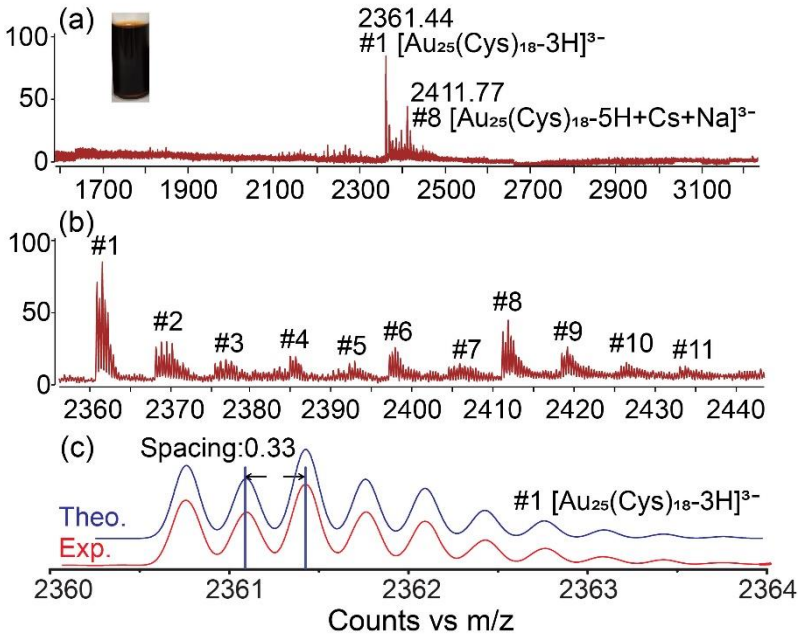

Figure 6. ESI mass spectra of synthesized $[Au_{25}(Cys)_{18}]$: (a) full-range spectra, (b) zoomed-in spectra in the *m/z* range of 2360-2440 and (c) comparison between theoretical and experimental isotope pattern of #1 peak of $[Au_{25}(Cys)_{18}]$ obtained with 10 mM initial $HAuCl_4$ concentration at residence time of 2.9 min, 80 °C, organic to aqueous flow ratio of 2 and cysteine to gold concentration ratio of 1.5. The insert in (a) shows the colour of the synthesized $[Au_{25}(Cys)_{18}]$ solution.

ESI-MS was used to confirm the composition of Au NCs formed. As shown in **Figure 6a**, ESI-MS showed the most intense set of peaks at *m/z* ~ 2361.4 in a range of 1500-5200, and an enlarged view of the spectrum in **Figure 6b** shows that the base peak at *m/z* 2361.4 (#1) was accompanied by a group of similar small peaks (#2 to #7) which correspond to H^+ dissociation and Na^+ coordination to $[Au_{25}(Cys)_{18}]$. Isotope pattern analysis of peak #1 in **Figure 6c** showed that the peak spacing between ^{12}C and ^{13}C was about 0.33. This indicated that $[Au_{25}(Cys)_{18}]$ carried three negative charges resulting in generation of $[Au_{25}(Cys)_{18}\text{-}3H]^{3-}$, and molecular weight (MW) was about 7083.2 Da. Other identifiable ionised species (#2 to #7) were (#2) $[Au_{25}(Cys)_{18}\text{-}4H+Na]^{3-}$ (MW 7106.1), (#3) $[Au_{25}(Cys)_{18}\text{-}5H+2Na]^{3-}$ (MW 7128.1 Da), (#4) $[Au_{25}(Cys)_{18}\text{-}6H+3Na]^{3-}$ (MW 7150.2 Da), (#5) $[Au_{25}(Cys)_{18}\text{-}7H+4Na]^{3-}$ (MW 7172.2 Da), (#6) $[Au_{25}(Cys)_{18}\text{-}8H+5Na]^{3-}$ (MW 7194.1 Da) and (#7) $[Au_{25}(Cys)_{18}\text{-}9H+6Na]^{3-}$ (MW 7216.2 Da) (see **Figure S7**). Additionally, other sets of cluster peaks (shown in the SI) were observed at *m/z* ~ 1808.6 and 2411, indicating 3^- and 4^- charged gas phase ions, and all of the peaks corresponded to $[Au_{25}(Cys)_{18}]$ dissociated with H^+ or coordinated with Na^+, K^+ or Cs^+ which are common contaminant ions in ESI-MS [32]. The results from ESI-MS combined with those from UV-Vis, show that atomically precise $[Au_{25}(Cys)_{18}]$ NCs were synthesized with high purity.

The spectra by matrix-assisted laser desorption ionization time-of-flight (MALDI-TOF) spectrometry (shown in **Figure S9**) also indicated high purity of the synthesized [$Au_{25}(Cys)_{18}$], as no other peaks were found in the range of *m/z* up to 15000. The yield of [$Au_{25}(Cys)_{18}$] determined by MP-AES was >90%, but there was no clear difference observed between the Au precursor (thiolate-Au(I) complexes) and the Au_{25} NCs after dialysis. Nevertheless, the yield of [$Au_{25}(Cys)_{18}$] was estimated with the optical density of the Au NCs solution at the 670 nm in the UV-Vis profile [10, 11], and the value of ~0.34 suggests a [$Au_{25}(Cys)_{18}$] yield of ~95% .

Through the above studies, it was demonstrated that it took only 3 min to synthesize high-purity Au_{25} NCs in the flow system at 80 °C with ten times (10 mM) the original concentration (1 mM) of the gold precursor compared to previously reported work in batch system [11]. The total throughput of the [$Au_{25}(Cys)_{18}$] in our flow system was increased to ~0.9 g_{Au}/day. To demonstrate the robustness of the developed process, a long term operation flow experiment was performed lasting 3 days. As can be seen by ESI-MS in **Figure 7**, the reactor system produced Au NCs of consistently high purity, throughout this period.

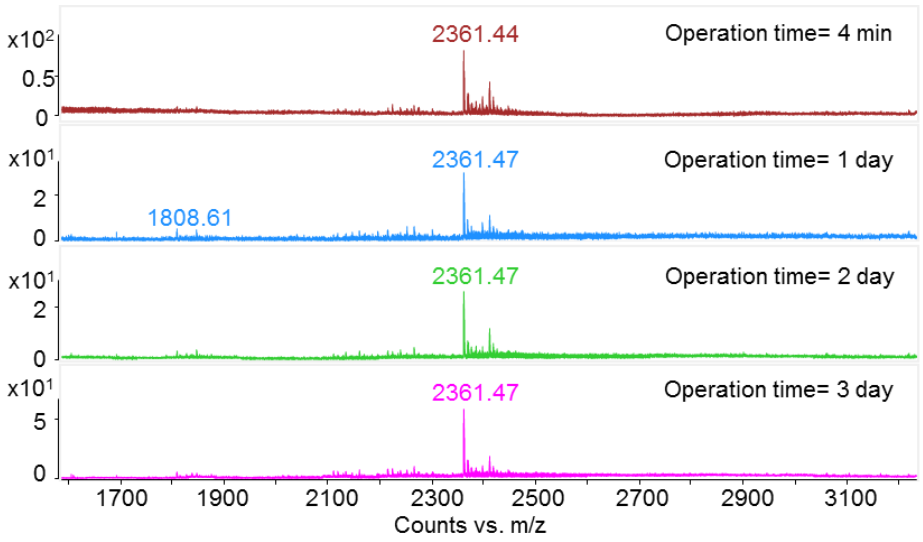

Figure 7. ESI mass spectra of synthesized [$Au_{25}(Cys)_{18}$] obtained with 10 mM initial concentration of gold precursor at different operation times (from 4 min to 3 days)**,** residence time of 2.9 min, 80 °C, organic to aqueous flow ratio of 2 and cysteine to gold precursor concentration ratio of 1.5.

Antimicrobial testing

Two samples of $[Au_{25}(Cys)_{18}]$ obtained from continuous operation times of 1-day and 3-days were used for photobactericidal enhancement of crystal violet treated silicone. Through a 24 h swell-encapusliation-shrink process, three types of silicone samples containing $[Au_{25}(Cys)_{18}]$ only, crystal violet only (CV) and crystal violet together with $[Au_{25}(Cys)_{18}]$ (CV& $[Au_{25}(Cys)_{18}]$) were prepared and they were tested against *Staphylococcus aureus,* which is Gram-positive bacterium, in white light. **Figure 8** shows the antimicrobial activity of the samples against *S. aureus* after 6 h incubation in white light. A reduction in the number of viable bacteria was not observed on the 1-day $[Au_{25}(Cys)_{18}]$, 3-day $[Au_{25}(Cys)_{18}]$ and CV samples compared to control (P-value >0.1). However, a statistically significant reduction was observed on the CV&1-day $[Au_{25}(Cys)_{18}]$, and CV&3-day $[Au_{25}(Cys)_{18}]$ samples (P-value <0.05). Compared to the control experiment, 1.78 and 1.66 log reductions were observed on CV&1-day Au NCs and CV&3-day $[Au_{25}(Cys)_{18}]$, respectively. Additionally, statistically significant difference between the CV&1-day $[Au_{25}(Cys)_{18}]$ and CV&3-day $[Au_{25}(Cys)_{18}]$ was not observed (P-value >0.1).

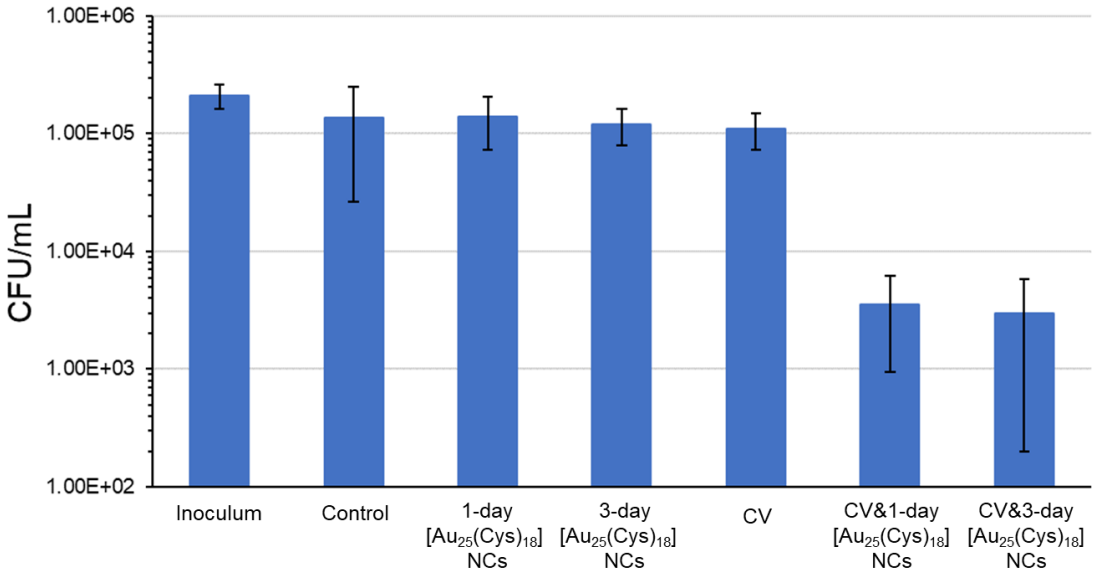

Figure 8 Antimicrobial activity of control, and treated silicone coupons after 6 h exposure of white light: Control, 1-day $[Au_{25}(Cys)_{18}]$, 3-day $[Au_{25}(Cys)_{18}]$, CV, CV&1-day $[Au_{25}(Cys)_{18}]$ and CV&3-day $[Au_{25}(Cys)_{18}]$ encapsulated silicone coupons. All experiments were performed with white light illumination of 312 lux at average temperature of 20 ^{o}C.

$[Au_{25}(Cys)_{18}]$ NCs are known to have intrinsic antimicrobial activity [29]. However, the NCs encapsulated in silicone did not exhibit antimicrobial activity. This might be because the number of the clusters encapsulated into the polymer was not enough to cause a reduction of bacterial viability. Despite the fact that crystal violet is a light-activated antimicrobial agent [33], the CV only encapsulated polymer did not show photobactericial activity after 6 h exposure of

white light. However, use of $[Au_{25}(Cys)_{18}]$ together with CV significantly enhanced photobactericidal activity. It is speculated that an interaction of $[Au_{25}(Cys)_{18}]$ and CV reinforces photochemical reactions, resulting in significant increase in the concentration of reactive oxygen species killing bacteria [34]. Through this antimicrobial test, it was confirmed that the 3-day synthetic process yielded stable quality of $[Au_{25}(Cys)_{18}]$.

In previous studies, it was shown that addition of 2 nm Au NPs into polymer containing crystal violet significantly enhanced photoactericidal activity [35, 36]. However, to obtain satisfactory performance, an intense white light source (>3300 lux) and high concentration of 2 nm Au NPs suspension (1000 mg/L) were required. In the present study, the solution used to prepare the antimicrobial silicone coupons contained only 35 mg/L $[Au_{25}(Cys)_{18}]$ and the white light intensity was ~312 lux. This indicates that the $[Au_{25}(Cys)_{18}]$ are more efficient at reinforcing photobactericial activity of crystal violet than 2 nm gold NPs.

4. Conclusion

A rapid synthesis of atomically precise $[Au_{25}(Cys)_{18}]$ nanoclusters (NCs) was demonstrated in a microfluidic segmented flow system. The mild reducing agent, CO, gave a gentle reduction environment and better control on the NCs synthesis. The utilization of a tube-in-tube set-up guaranteed that the CO was contained inside the tube, resulting in a much safer synthetic procedure. Compared to typical reaction times of few hours or even days in batch systems, operation at elevated temperature accelerated the size evolution and significantly shortened the total reaction time to as little as 3 min with high purity and yield. In addition, the throughput could be increased to 0.9 g_{Au} per day, and the process was shown to provide consistent quality gold NCs over a period of 3 days. These results demonstrate a high potential for translation of this method to an industrial enviroment. Regarding the application of $[Au_{25}(Cys)_{18}]$, it was oberved that Au NCs addition reinforced significantly the photobactericidal activity of crystal violet encapsulated silicone against *S. aureus* in white light. This indicates that $[Au_{25}(Cys)_{18}]$ can reinforce bactericidal activity of photosensitizer surfaces at lower concentration (35 mg/L vs. 1000 mg/L) and light intensity (312 Lux vs. 3300 Lux) compared to 2 nm gold NPs, and hence are more economical for antimicrobial application to prevent contamination of hospital surfaces.

Acknowledgements

This work was supported by EPSRC (grant EP/M015157/1). HH acknowledges the financial support from the program of UCL-CSC Joint Scholarship. This research has been performed with the use of facilities at the Research Complex at Harwell including MP-AES equipment. The authors would like to thank the Research Complex for access and support to equipment.

The authors gratefully acknowledge support for SAXS measurements from the EPSRC “Frontier Engineering” Centre for Nature Inspired Engineering (EP/K038656/1). We also would like to thank Dr Christopher Windle (University College London) for his support with the IR measurements.

References

[1] R. Jin, C. Zeng, M. Zhou, Y. Chen, Atomically precise colloidal metal nanoclusters and nanoparticles: Fundamentals and opportunities, Chem. Rev. 116 (2016) 10346-10413.

[2] T.G. Schaaff, G. Knight, M.N. Shafigullin, R.F. Borkman, R.L. Whetten, Isolation and selected properties of a 10.4 kDa gold: Glutathione cluster compound, J. Phys. Chem. B 102 (1998) 10643-10646.

[3] M.H. Muhammed, T. Pradeep, Luminescent Quantum Clusters of Gold as Bio-labels, Advanced Fluorescence Reporters in Chemistry and Biology II, Springer 2010 pp. 333-353.

[4] F.P. Zamborini, J.F. Hicks, R.W. Murray, Quantized double layer charging of nanoparticle films assembled using carboxylate/(Cu^{2+} or Zn^{2+})/carboxylate bridges, J. Am. Chem. Soc. 122 (2000) 4514-4515.

[5] G. Li, R. Jin, Atomically precise gold nanoclusters as new model catalysts, Acc. Chem. Res. 46 (2013) 1749-1758.

[6] Y. Shichibu, Y. Negishi, H. Tsunoyama, M. Kanehara, T. Teranishi, T. Tsukuda, Extremely high stability of glutathionate‐protected Au_{25} clusters against core etching, Small 3 (2007) 835-839.

[7] X. Kang, H. Chong, M. Zhu, $Au_{25}(SR)_{18}$: The captain of the great nanocluster ship, Nanoscale 10 (2018) 10758-10834.

[8] M. Brust, M. Walker, D. Bethell, D.J. Schiffrin, R. Whyman, Synthesis of thiol-derivatised gold nanoparticles in a two-phase liquid-liquid system, J. Chem. Soc., Chem. Commun. (1994) 801-802.

[9] C.J. Murphy, T.K. Sau, A.M. Gole, C.J. Orendorff, J. Gao, L. Gou, S.E. Hunyadi, T. Li, Anisotropic metal nanoparticles: Synthesis, assembly, and optical applications, J. Phys. Chem. B 109 (2005) 13857-13870.

[10] Y. Negishi, K. Nobusada, T. Tsukuda, Glutathione-protected gold clusters revisited: Bridging the gap between gold(I)−thiolate complexes and thiolate-protected gold nanocrystals, J. Am. Chem. Soc. 127 (2005) 5261-5270.

[11] Y. Yu, Z. Luo, Y. Yu, J.Y. Lee, J. Xie, Observation of cluster size growth in CO-directed synthesis of $Au_{25}(SR)_{18}$ nanoclusters, ACS Nano 6 (2012) 7920-7927.

[12] Z. Wu, J. Suhan, R. Jin, One-pot synthesis of atomically monodisperse, thiol-functionalized Au_{25} nanoclusters, J. Mater. Chem. 19 (2009) 622-626.

[13] R. Jin, H. Qian, Z. Wu, Y. Zhu, M. Zhu, A. Mohanty, N. Garg, Size focusing: a methodology for synthesizing atomically precise gold nanoclusters, The Journal of Physical Chemistry Letters 1 (2010) 2903-2910.

[14] T. Chen, Q. Yao, X. Yuan, R.R. Nasaruddin, J. Xie, Heating or cooling: Temperature effects on the synthesis of atomically precise gold nanoclusters, J. Phys. Chem. C 121 (2017) 10743-10751.

[15] H. Qian, R. Jin, Controlling nanoparticles with atomic precision: The case of $Au_{144}(SCH_2CH_2Ph)_{60}$, Nano Letters 9 (2009) 4083-4087.

[16] S.K. Katla, J. Zhang, E. Castro, R.A. Bernal, X.J. Li, Atomically-precise $Au_{25}(SG)_{18}$ nanoclusters: Rapid single-step synthesis and application in photothermal therapy, ACS Appl. Mater. Interfaces 10 (2018) 75-82.

[17] X. Yuan, B. Zhang, Z. Luo, Q. Yao, D.T. Leong, N. Yan, J. Xie, Balancing the rate of cluster growth and etching for gram‐scale synthesis of thiolate‐protected Au_{25} nanoclusters with atomic precision, Angew. Chem. 126 (2014) 4711-4715.

[18] Z. Luo, V. Nachammai, B. Zhang, N. Yan, D.T. Leong, D.-e. Jiang, J. Xie, Toward understanding the growth mechanism: Tracing all stable intermediate species from reduction of Au(I) – thiolate complexes to evolution of Au_{25} nanoclusters, J. Am. Chem. Soc. 136 (2014) 10577-10580.

[19] P.W. Stone, Economic burden of healthcare-associated infections: an American perspective, Expert Rev. Pharmacoecon. Outcomes. Res. 9 (2009) 417-422.

[20] D.J. Weber, D. Anderson, W.A. Rutala, The role of the surface environment in healthcare-associated infections, Curr. Opin. Infect. Dis. 26 (2013) 338-344.

[21] G. Wu, E. Cao, S. Kuhn, A. Gavriilidis, A novel approach for measuring gas solubility using a tube-in-tube membrane contactor, Chem. Eng. Technol. 40 (2017) 2346-2350.
[22] R.W. Cargill, "Solubility data series." *Carbon monoxide.*, Pergamon Press, Oxford, 1990.
[23] L. Yang, K.F. Jensen, Mass transport and reactions in the tube-in-tube reactor, Org. Process Res. Dev. 17 (2013) 927-933.
[24] E. López-Guajardo, E. Ortiz-Nadal, A. Montesinos-Castellanos, K.D. Nigam, Coiled flow inverter as a novel alternative for the intensification of a liquid-liquid reaction, Chem Eng Sci 169 (2017) 179-185.
[25] I. Chakraborty, T. Pradeep, Atomically precise clusters of noble metals: Emerging link between atoms and nanoparticles, Chem. Rev. 117 (2017) 8208-8271.
[26] T. Schaaff, M. Shafigullin, J. Khoury, I. Vezmar, R. Whetten, W. Cullen, P. First, C. Gutierrez-Wing, J. Ascensio, M. Jose-Yacaman, Isolation of smaller nanocrystal Au molecules: Robust quantum effects in optical spectra, J. Phys. Chem. B 101 (1997) 7885-7891.
[27] Y. Yu, J. Li, T. Chen, Y.N. Tan, J. Xie, Decoupling the CO-reduction protocol to generate luminescent $Au_{22}(SR)_{18}$ nanocluster, J. Phys. Chem. C 119 (2015) 10910-10918.
[28] M. Wuithschick, A. Birnbaum, S. Witte, M. Sztucki, U. Vainio, N. Pinna, K. Rademann, F. Emmerling, R. Kraehnert, J. Polte, Turkevich in new robes: Key questions answered for the most common gold nanoparticle synthesis, ACS Nano 9 (2015) 7052-7071.
[29] K.Y. Zheng, M.I. Setyawati, D.T. Leong, J.P. Xie, Antimicrobial gold nanoclusters, ACS Nano 11 (2017) 6904-6910.
[30] Y. Bao, Interaction between Au_{25} monolayer protected clusters with lipid nanodiscs, University of Connecticut, 2015.
[31] M. Azubel, J. Koivisto, S. Malola, D. Bushnell, G.L. Hura, A.L. Koh, H. Tsunoyama, T. Tsukuda, M. Pettersson, H. Häkkinen, R.D. Kornberg, Electron microscopy of gold nanoparticles at atomic resolution, Science 345 (2014) 909-912.
[32] B.O. Keller, J. Sui, A.B. Young, R.M. Whittal, Interferences and contaminants encountered in modern mass spectrometry, Anal. Chim. Acta 627 (2008) 71-81.
[33] G.B. Hwang, E. Allan, I.P. Parkin, White light-activated antimicrobial paint using crystal violet, ACS Appl. Mater. Interfaces 8 (2016) 15033-15039.
[34] S. Noimark, E. Salvadori, R. Gomez-Bombarelli, A.J. MacRobert, I.P. Parkin, C.W.M. Kay, Comparative study of singlet oxygen production by photosensitiser dyes encapsulated in silicone: towards rational design of anti-microbial surfaces, Phys. Chem. Chem. Phys. 18 (2016) 28101-28109.
[35] T.J. Macdonald, K. Wu, S.K. Sehmi, S. Noimark, W.J. Peveler, H. du Toit, N.H. Voelcker, E. Allan, A.J. MacRobert, A. Gavriilidis, I.P. Parkin, Thiol-capped gold nanoparticles swell-encapsulated into polyurethane as powerful antibacterial surfaces under dark and light conditions, Sci. Rep. 6 (2016) 39272.
[36] S. Noimark, E. Allan, I.P. Parkin, Light-activated antimicrobial surfaces with enhanced efficacy induced by a dark-activated mechanism, Chem. Sci. 5 (2014) 2216-2223.